Journal of Materials Chemistry A

Accepted Manuscript

ROYAL SOCIETY OF CHEMISTRY

www.rsc.org/materialsA

A Simple All-solution Approach to the Synthesis of Large ZnO Nanorod Networks

A. Resmini[1], I. G. Tredici[1], C. Cantalini[2], L. Giancaterini[2], F. De Angelis[3], E. Rondanina[3], M. Patrini[4], D. Bajoni[5], U. Anselmi-Tamburini[1,*]

[1]Department of Chemistry, University of Pavia, Viale Taramelli 12, I-27100 Pavia, Italy.

[2]Department of Industrial Engineering, University of L'Aquila, Via Gronchi 18, I-67100 L'Aquila, Italy

[3]Department of Nanostructures, Italian Institute of Technology, Via Morego 30, I-16163 Genova, Italy

[4]Department of Physics, University of Pavia, Via Bassi 6, I-27100 Pavia, Italy

[5]Department of Industrial and Information Engineering, University of Pavia, Via Ferrata 1, I-27100 Pavia, Italy

**corresponding author: tau@unipv.it*

Abstract

ZnO nanorods present a great potential for application in optical, sensing and piezoelectric devices thanks to their nanometric diameter and large surface area. In some of these applications a probing current must flow directly through the nanorods, requiring each nanorod to be directly connected to two electrodes. To attain this architecture few solutions have been proposed in the past, mostly involving the use of complex and time-consuming procedures, but the large-scale production of such devices represents still a major challenge. We present here a new all-solution approach that allows the fabrication of extensive self-assembled, bi-dimensional networks of ZnO nanorods. Such networks can be easily produced on interdigitated electrodes with no need for any alignment, resulting directly in the formation of very robust devices. The entire process is fast, does not require any complex experimental apparatus and involves only the use of inexpensive and environmentally benign chemical reagents. We demonstrate the potentiality of such networks in a gas sensing application, where these networks resulted to be able to detect NO_2 at trace levels, at low temperature, using UV-visible activation.

Keywords

ZnO nanorod, patterning, hydrogels, hydrothermal growth, gas sensing

1. Introduction

Nanostructures of semiconducting metal oxides have been extensively investigated in the past few years because of their technologically relevant characteristics. Nanostuctures of ZnO have been object of particular attention because of the unique properties and ease of synthesis of this compound. ZnO presents in fact a noteworthy combination of physical and chemical properties: a wide direct band gap (3.37 eV), piezoelectric properties and a high sensitivity towards several chemical species. As a result, ZnO finds wide application in field-emitting devices,[1] piezogenerators,[2,3] field-effect transistors (FET),[4,5] dye-sensitized solar cells (DSSC),[6-9] UV lasers,[10,11] light-emitting diodes (LED) and chemical as well as biological sensors.[12-15] Nanorods (NRs) of ZnO have been synthesized using a variety of methods, including carbothermal reduction, gas deposition, metal-organic chemical vapor deposition, laser ablation and wet chemical methods.[16] These last approaches have been receiving a growing attention as they involve the use of simple experimental apparatuses, low process temperatures and environmentally friendly chemicals.[17-20] Wet-chemical methods include electrodeposition,[21] solvothermal[22] and hydrothermal growth, the latter being the most diffused for the synthesis of ZnO NRs, since it does not require any particular apparatus and does not involve the use of toxic solvent or high temperature.[23] Hydrothermal synthesis of ZnO NRs employing zinc salts as sources of cations and sodium hydroxide[24] or ammonia,[25,26] as well as easily-hydrolisable amines such as urea or hexamethylenetetramine, have been widely reported.[27-30] More recently, the use of organic surfactants, such as polyethyleneimine (PEI), has been introduced to further orient the nucleation of ZnO, by virtue of their ability to preferentially adsorb onto the lateral non-polar surfaces of growing NRs.[25,26,31] Using these approaches long ZnO NRs presenting length above 10 micrometers and aspect ratio above 100 can be achieved, although a

refilling of growth solution is usually required after a couple of hours.[32] Only few reports demonstrated the possibility of obtaining such long and narrow ZnO NRs through one-pot hydrothermal syntheses.[33]

In several applications NRs present some advantages over nanocrystalline thin films, however the large-scale fabrication of devices based on ZnO NRs represents still a major challenge. In most reported applications the NRs are grown on top of a countinous film that is directly in contact with the electrodes.[21,32] In sensing applications this configuration does not take full advantage of the NRs characteristics, as the probing current is mostly confined in the basal film, with the NRs producing only an indirect influence on its response. In order to take full advantage of the NRs geometry the probing current should flow directly through them. Examples of this architecture has been reported in few cases, but it has been mostly realized through a *pick-and-place* approach, in which a single NR or, more commonly, a large number of them, are detached from the substrate where they have been primarily grown and repositioned on other substrates provided with metallic electrodes.[34,35] When applied to a single NR this method results to be extremely time consuming and presents some interest only for basic research applications. Much more viable is the use of large number of NRs suspended in a solvent and then dispersed on a substrate, but this approach usually produces a low density network of NRs that is poorly reproducible and presents poor connection with the metallic electrodes and among the NRs themselves.[36,37]

An alternative and more promising approach for large scale applications is represented by the synthesis of a network of interconnected NRs grown from appropriately patterned seed layers directly connected to the metallic electrodes. When properly designed, this approach can take advantage of the self-organizing characteristics of these nanostructures, resulting in a minimum number of fabrication steps. Few examples of simple, one dimensional

networks of NR have been reported in the literature, mostly related to the realization of field-effect transistors (FET),[38,39] UV detectors,[40] and gas sensors.[41,42] However, most of them do not involve the use of solution-grown NRs,[38-40] and none the use of patterning techniques different from photolithography.

In this work we present a simple all-solution approach to the realization of complex, tri-dimensional, self-assembled network of ZnO NRs obtained through an optimized hydrothermal growth of long NRs onto a patterned ZnO seed-layer. The latter was produced through an optimized soft-lithographic approach involving an hydrogel-based precursor. The NRs networks obtained through this method can easily be grown over interdigitated electrodes presenting a pitch of at least few micrometers, with no need for alignment between the electrodes and the seeding pattern. The whole architecture can be obtained using an extremely simple experimental apparatus and is all based on solution processes involving the use of inexpensive and environmentally friendly chemicals.

2. Results and Discussion

A schematic representation of the overall process for the synthesis of bi-dimensional, large-networks of ZnO NRs on a generic substrate is reported in Figure 1a. The network of interconnected NRs is obtained using a seeding pattern of micrometric pillars of ZnO. The patterning procedure used for the synthesis of these micropillars followed to some extent an approach we presented in a previous paper[43] and is based on the use of a metal-loaded hydrogel as a precursor.[44-46] After deposition of a hydrogel precursor solution (ii), a PDMS mold is cast on the liquid film (iii); a load of 100 kPa is applied over the mold, and the film is polymerized in few minutes by UV irradiation (iv). After the mold removal, the obtained

patterned hydrogel (v) undergoes a thermal degradation at 500 °C, yielding a pattern of ZnO micropillars (vi), which is then used as a seed layer for the hydrothermal growth of the NRs network (vii).

The same simple procedure can be applied with no modifications on substrates presenting metallic interdigitated electrodes. A schematic of a network of ZnO NRs synthesized on this kind of substrates is shown in Figure 1b, which highlights how the purpose of providing an electrical path between two electrodes can be efficiently fulfilled by the bi-dimensional network of inter-connected ZnO NRs, grown from neighboring ZnO pillars. The inset of Figure 1b shows the good contact existing between adjacent NRs, which result to be partially compenetrated.

2.1. Patterning of the seeding layers.

As mentioned above, the first stage of the process is represented by the synthesis of the micropillars of nanocrystalline ZnO, which will then act as seeding for the subsequent growth of the NRs network. The good outcome of this first step, in terms of patterning quality, is therefore crucial for the entire process: Figure 2 shows the results obtained at this stage of the procedure. After removal of the PDMS mold, a high quality pattern of prisms made out of solid Zn-loaded hydrogels is obtained (Figure 2a). The base dimensions of the prisms are 3.5x3.5 μm, while their height is about 10 μm. The spacing between the prisms was about 6 μm. Upon thermal treatment the organic matrix is degraded and the Zinc ions dissolved in the hydrogel convert into ZnO. The process is accompanied by a significant contraction in molar volume. This volume contraction is mostly adjusted through a

reduction in the micropillars height, but a significant lateral shrinkage is also observed. Figure 2b and 2c show the pattern at the end of the degradation process. Small 1x1x2 μm pillars of ZnO are here observed. They appear to be slightly deformed as a result of the large volume contraction associated to the process. The pillars are polycrystalline and characterized by a grain size of about 15-20 nm. As a result of the lateral shrinkage produced by the thermal degradation the distance between the micropillars is increased to about 8 μm. The design of the pattern was accurately planned to assure an efficient electrical contact, once that the NRs are grown. Taking into account the lateral shrinkage associated to the degradation process (which was modeled on several patterns with different geometries), we planned a final distance between adjacent pillars of about 8 μm, a dimension comparable with the expected maximum length of our NRs (about 10 μm) and allowing an effective bridging between neighbor pillars even in presence of a significant tilting angle.

Although presenting some slight deformation, the quality of the lithographic process appears to be excellent, despite the large decrease in molar volume associated with the degradation process. The patterns result to be uniform and defect free over large areas, up to several square millimeters. It must also be noted the complete absence of any residual film between the micropillars even when inexpensive and untreated microscope glass slide are used as a substrate.

2.2. Growth of the ZnO NRs network.

The next step of the process is represented by the hydrothermal growth of the network of ZnO NRs. We optimized a hydrothermal synthesis allowing the growth of ZnO NRs with

high length-over-diameter ratio. This synthesis employs zinc nitrate as a source of cations, and hexamethylenetetramine (HMT) as a base in presence of ammonium hydroxide and polyethylenimine (PEI). Zinc nitrate and HMT are widely employed as sources of Zn^{2+} and NH_3, respectively. The latter serves as a base for the production of OH^-, which in turn forms the soluble tedrahedral $Zn(OH)_4^-$ complex through the reaction $Zn^{2+} + 4OH^- \rightleftharpoons Zn(OH)_4^-$. Such complex is involved in the nucleation of ZnO at the interface of the seed-layers grains exposing their (0001) face to the solution of growth. This process results in the formation of the primordial ZnO NRs through the reaction $Zn(OH)_4^- \rightleftharpoons ZnO + H_2O + 2OH$.[47-48] the growth rates V of the exposed surfaces of ZnO NRs are known to follow the order $V(0001) > V(10\bar{1}0) > V(10\bar{1}\bar{1}) > V(10\bar{1}1)$, primordial NRs tend to growth preferably along their *c*-axis [0001] over the entire hydrothermal reaction, achieving a large aspect ratio (length/diameter).[18]

Although ammonia is formed through the hydrolysis of HMT, an additional amount of ammonia has been introduced in the growth solution to help suppressing the homogeneous nucleation of ZnO.[33,49] Ammonia, in fact, forms complexes with the zinc ions, $Zn^{2+} + nNH_3 \rightleftharpoons Zn(NH_3)_n^{2+}$ (n=1, 2, 3, 4), lowering the concentration of free Zn^{2+} in the solution. Since the homogeneous nucleation of ZnO usually requires a higher level of supersaturation in respect to the heterogeneous nucleation, an accurate choice of the ammonia concentration results in the suppression of the homogeneous nucleation, maintaining the possibility of heterogeneous nucleation. The addition of a large amount of ammonia, however, may also cause a decrease of the NRs' growth rate due to the resulting decrease in the concentration of free Zn^{2+}. To avoid this effect polyethyleneimine (PEI) has been added to the solution. PEI is a well-known organic non-polar surfactant usually added to limit the growth in width of ZnO NRs by virtue of its tendency to interact preferably with non-polar lateral surfaces

of ZnO NRs, reducing their lateral growth.[25-26,31] In this case, the presence of PEI helps to limit the growth of the homogeneously formed small nuclei of ZnO by adsorbing onto their surfaces and causing in turn their re-dissolution. This reduces the need of employing high ammonia concentrations.[33] The suppression of the homogeneous nucleation is of primary importance if long and narrow ZnO NRs need to be grown. In fact, the occurrence of homogeneous nucleation decreases the concentration of Zn^{2+} in the solution, resulting in a NRs lower growth rate.

The optimization of the hydrothermal reaction through a fine tuning either of the concentrations of the chemicals and of the reaction temperature allowed to obtain long and narrow ZnO NRs presenting high aspect ratio (~100) and large length of about 10 micrometers. Such morphological features of ZnO NRs obtained allowed filling the distances between different ZnO pillars of the patterned seed-layer as well as to form a large number of junctions between touching NRs, which is required for electrical connection over the network of nanostructures.

Figure 3 illustrates the very early stages of the process. Figure 3a shows as the NRs appear to originate from the nanograins that constitute the micropillars and grow perpendicularly to their surfaces (Figure 3b). As the hydrothermal process goes on, both NRs length and diameter are increased, although at very different rates due to the different growth rates of top and lateral surfaces of NRs. The gradual increase in NRs diameter appears to be accompanied by a decrease in the NRs density, indicating the possibility of merging of neighbor NRs during the process. Further evolution is shown in Figure 4 and Figure 5, which depict respectively the top-views and cross-sections of the NRs networks grown at zero (a), 135 (b), 180 (c), and 300 min (d). Here a gradual increase in the NRs length (and diameter) is observed (Figure 4b-d and 5b-d) until the NRs tips begin touching

and forming well-developed connections, as can be observed in the micrographs reported in Figure 6.

NRs networks characterized by these morphologies have been obtained with excellent uniformity and reproducibility on areas of several square millimeters, as shown in Figure 4b-d. It must be noted as only NRs originating from the pillars are observed (Figure 5b-d, Figure 6a) and no growth on the substrate between the pillars is detected at any stage of the process. This assures that the NRs junctions provide the only conduction path existing between the micropillars. As mentioned above, these junctions appeared to be particularly robust; in most cases, in fact, the NRs appear to be intercrossing each other and not just touching on their surfaces (Figure 6b).[50-51]

The number of NRs junctions appears to increase with the NRs length, as can be inferred by comparing the top-views of Figure 4c and 4d and the relative of Figure 5c and 5d. This observation suggests the possibility that the overall electrical conductivity of the NRs network can be easily controlled through a modification of the parameters that influence the NRs growth, such as the reaction time, the concentration of chemicals and the temperature. Because of these characteristics no further heat treatment is required to improve the conductivity of the NRs network at the end of the process, as often required in the case of networks obtained by deposition of NRs suspended in a solvent.[36,37]

The entire deposition process can be reproduced with no modifications on substrates provided with metallic electrodes, allowing the direct realization of actual microdevices (Figure 7). Figure 7a shows an example of ZnO seeding micropillars obtained on a silicon nitride substrate presenting interdigitated Pt electrodes. The inset remarks how the lithographic process can produce high quality results independently from the nature of the substrate: the pillar printed across the border between the SiN substrate and the Pt track

appears to be perfectly symmetrical and defect-free. A further advantage of this architecture appears evident from the figure: no alignment is required between the electrodes and the micropillars, in order to develop a conduction path. As explained by the schematics reported in Figure 7b, as long as the distance between the micropillars (A) is smaller that the distance between the Pt lines (B), the formation of a conduction path connecting two lines through a network of ZnO NRs is always possible, regardless the orientation of the pattern; this is a characteristic that considerably simplifies the realization of an actual device.

2.3. Characterizations of the networks of ZnO NRs.

Figure 8a shows the XRD of a full-grown network of ZnO NRs similar to the one reported in Figure 4d. The pattern shows the well-crystallized nature of the material that presents only the peaks corresponding to the Zincite hexagonal crystal structure. The relative intensity of the peaks is substantially altered when compared with a standard powder pattern (reported as a reference in Figure 8a); the peak corresponding to the basal plane (0002) is strongly enhanced as a result of the preferred orientation of the NRs along the c-axis.

Figure 8b shows the photoluminescence (PL) spectrum, collected at room temperature, for a typical as-grown NRs network. A major emission peak corresponding to the near-band-edge (NBE) results evident at 380 nm, together with the related small emission signal at twice its wavelength, ascribed to the second order diffraction of the NBE emission.[52-55] A weak emission band in the visible region between 500 and 700 nm is also evident, usually discussed in terms of overlapping “green” and “orange” components due to oxygen vacancies, surface states, or structural defects.[57-58] However, such visible emission band is only hardly visible in comparison with the UV emission band.[59] The absence of this band is

generally considered as an indication of the good crystal quality of the ZnO nanostructures.[57]

With the purpose of testing the presence of electrical connection between the NRs we tested the electrica response of the network deriving from its exposure to NO_2. Gas concentrations between 200 and 800 ppb and UV irradiation with a light source characteized by a λ_{max} of 430 nm and at different temperatures (25, 50, and 75 °C) have been used (Figure 8c).

The sensitivity response (SR) of the device as represented by the function SR (%) $=[(R_g-R_a)/R_a)]\cdot 100$, where R_g indicates the network resistance in NO_2 and R_a its resistance in air (base line resistance). Table 1 shows the SR at different operating temperatures and different gas concentrations. It is evident as higher operating temperature result in better values of SR for all the investigated gas concentration. Several NO_2 gas response tests have been carried out and the SRs uncertainty has been reported in Table 1.

Gas adsorption/desorption is reversible, indicating a complete recovery of the base line that appears to be more complete at higher operating temperatures (i.e. 75°C), as reported in Figure 8c.

The resistance increase observed upon NO_2 exposure confirms an *n*-type response, in agreeement with previous research.[60] The surprisingly low resistance in dry air, which ranges between 70 and 90 Ohm when the device is illuminated at a 430 nm wavelenght in the 25-75 °C temperature range, provides a clear evidence for the occurrence of extended, well developed connections between the bridging self-assembled NRs. These conductivity values are at least two orders of magnitude higher of the one obtained under the same experimental conditions using thin films, nanolines and calcined ZnO powders exposed to UV-LED irradiation.[61,62] This feature derives from the peculiarity of the produced

nanostructure, composed by well crystallized NRs, presenting a large number of connections and a strong bonding with the electrodes. The overall dimension of the network, that extends without interruptions on the whole surface covered by the interdigitated electrods (5 x 5 mm), contributes to producing a low baseline resistance. The data of Figure 8c also indicate that our NRs network is able to recognize the presence of NO_2 oxidizing gas at very low concentration values. A quite limited comparison with previously reported devices based on NRs networks can be performed in the case of NO_2 gas as a target analyte. Only few of these devices have been described in the literature[41,42,63] and only in two cases the sensing material was ZnO,[41,42] but none of these examples involved a low temperature detection in presence of UV or visible activation.

In dry air and dark conditions oxygen species such as O^{2-}, O^-, O_2^- are known to be adsorbed on the surface of metal oxides, with the latter being predominant at room temperature.[64] The formation of $O2^-_{ads}$ involves the capture of free electrons in the conduction band through the reaction:

$$O2_{phys} + e' \rightleftharpoons O2^-_{ads}$$

A depletion layer is formed at the surface of the metal oxide, which in turn increases the resistance of the sensor. When the oxygen partial pressure or the temperature varies, $O2^-_{ads}$ may be released forming $O_{2\,phys}$ or even $O_{2\,gas}$ and e'. It was suggested that at conventional operating temperatures upon exposure to NO_2 gas in dark conditions , the bound electron from the adsorbed oxygen species $O2^-_{ads}$ might be transferred to the physisorbed NO_2 through the reaction:

$$NO2_{phys} + O2^-_{ads} \rightleftharpoons NO2^-_{ads} + O2_{phys}$$

When the physisorbed NO_2 accepts electrons from $O_2^-{}_{ads}$, the stable chemisorbed $NO_2^-{}_{ads}$ state is created. It is well known that $NO_2^-{}_{ads}$ forms surface acceptor levels deeper than oxygen ion $O_2^-{}_{ads}$ and increases the thickness of depletion layer. However, at room temperature in dark conditions, $O_2^-{}_{ads}$ is stable and $NO_{2\,phys}$ molecules do not easily extract bound electrons from $O_2^-{}_{ads}$ to form $NO_2^-{}_{ads}$.[65,66] UV irradiation strongly enhances the chemisorption of NO_2 at low temperature, improving the NO_2 sensing response. As it has been suggested, holes and electrons photogenerated through a band-to-band excitation might induce either the release of $O_2^-{}_{ads}$ or formation of $NO_2^-{}_{ads}$, according to the following reactions:

$$O_2^-{}_{ads} + h^{\bullet} \rightleftharpoons O_{2\,gas}$$

$$NO_{2\,phys} + e' \rightleftharpoons NO_2^-{}_{ads}$$

The strong influence of UV radiation on the sensitivity and response time of semiconducting oxides has been intensively investigated only recently.[61,62,66-68] In our case the energy of the radiating source is too low to photogenerate electron-hole couples, as its wavelenght (430 nm) is well above the intrisic absorption edge for ZnO, located at 380 nm. However, recently it has been pointed out that electrons in the valence band of ZnO can be promoted to the conduction band by lower energy photons through two- or multi-photon processes.[62] These generated holes can then interact with the chemically adsorbed oxygen molecules, promoting their desorption and producing free adsorption sites for the target molecules. As evidenced in Figure 8d, however, the resistance of the sample at 25 °C in dark conditions is only twice of the resistance of the irradiated sample. This again indicates that the elevated conductivity of our samples is primarily related to the extended

interconnectivity between the elements of the NRs network and to their good connection with the Pt electrodes.

3. Experimental section

3.1. Patterning of ZnO seed layers.

A polymeric hydrogel precursor was obtained by mixing poly(ethylene glycol)dimethacrylate (PEG-DMA, Mn 550) with a cross-linker (trimethylolpropane benzoate diacrylate), methanol as a solvent and 2,2-dimethoxy-2-phenylacetophenone as photoinitiator. Zinc ions were added to the hydrogel by dissolving $Zn(NO_3)_2 \cdot 6\ H_2O$ in the precursor solution. A typical precursor mixture contained methanol (30% wt.), PEG-DMA (40% wt.), trimethylolpropane benzoate diacrylate (8% wt.), photoinitiator (10% wt.), and $Zn(NO_3)_2 \cdot 6\ H_2O$ (7% wt.), corresponding to a zinc concentration of 0.30 M. All these chemicals were purchased from Sigma-Aldrich and used as received. The substrates were microscope glass slides, silicon and silicon nitride wafers, some of them provided with interdigitated Pt electrodes. Before use they were cleaned with acetone (99.8% wt.), dried at 200 °C on a hot plate for 5 min. Few drops of the precursor solution were placed onto the substrate and then patterned through a soft-lithographic approach using a polydimethylsiloxane (PDMS) mold. The mold was obtained by pouring a previously outgassed mixture with a 10:1 ratio of elastomer Sylgard 184 and its curing agent (Dow Corning) onto a silicon master and thermally curing it at 60 °C for 24 h. The silicon master presented a pattern of small pillars 5x5 μm wide and 10 μm high. It was produced by photolithography on a P-type Silicon wafer (500 μm thick). The photolithographic process was performed using an AZ 5214-E resist and a laser writer DWL 66FS (Heidelberg

Instruments) operated at 0.4 mW, followed by an inductively coupled plasma-reactive-ion etching (ICP-RIE) realized using a SI 500 plasma etcher (Sentech Instruments GmbH) through Bosch process, using SF_6, Ar and C_4F_8 gases. The preparation of the silicon master was performed only once for each geometry, as a large number of PDMS molds can be replicated from each master. The soft-lithographic procedure was completed by applying a pressure of 100 kPa on the PDMS mold, that was left on the substrate overnight. The assembly was then irradiated with UV (λ_{max} = 310 nm) for 20 min, converting the precursor solution into a solid Zn–loaded hydrogel. The pressure was then released and the substrate was heated on a hot plate at 90 °C for 30 min. The PDMS mold was peeled off leaving a pattern of squared pillars of Zn-loaded hydrogel on the substrate. The hydrogel was then thermally degraded in static air at 500 °C for 60 min producing a pattern of nanostructured ZnO micropillars.

3.2. Hydrothermal growth of ZnO NRs networks.

Networks of ZnO NRs were obtained through hydrothermal processes using the previously obtained ZnO micropillars as seeding. The solution for the hydrothermal growth was composed by $Zn(NO_3)_2 \cdot 6\ H_2O$ (0.25 mM), ammonium hydroxide (650 mM), HMT (0.25 mM), PEI (2.24 mM) and deionized water. The Zn nitrate solution was added drop-wise under continuous stirring to a solution containing the bases. The final mixture was poured into a Duran® GL45 100 ml laboratory glass bottle and the substrate with the patterned ZnO seed-layer was positioned at the bottom. The hydrothermal treatment was carried out at 90 °C for 135, 180 and 300 min. Finally, the substrate was retrieved, rinsed with deionized water and dried at room temperature.

3.3. Structural characterization.

XRD measurements were performed by using a Bruker D8 Advance diffractometer equipped with a Cu anticathode ($\lambda_{CuK\alpha}$ = 1.541838 Å), operated at 40 kV and 40 mA. A thin film stage and a soller slit on the diffracted beam were used. XRD patterns were collected using a 6.5 ° incident angle, with a step of 0.02 ° and an acquisition time of 5 s per step.

3.4. Microstructural characterization.

HR-SEM measurements were performed by using a TESCAN MIRA 3 XMU Microscope, operated at 30 kV on samples previously coated with graphite (Cressington carbon coater 108carbon/A).

3.5. Optical characterization.

Photoluminescence spectra were measured by exciting the samples with a 355 nm frequency tripled Nd:YAG laser (PowerChip NanoUV 355 by Teem Photonics, maximum power 12 mW) and collecting the emitted light in reflection configuration. The laser beam was focused to a 0.5 mm diameter spot onto the sample surface. A 355 RazorEdge ultra steep long-pass edge filter by Semrock was used to reject stray light from the laser pump. Finally, the signal was sent to a monochromator (Acton SP-2300, Princeton Instruments) coupled to a liquid nitrogen-cooled Silicon CCD (Spec-10, Princeton Instruments).

3.6. Electrical characterization.

Gas sensing measurements were carried out on samples that have been grown on a on 5x5 mm SiO_2/Si_3N_4 substrate, presenting on one side 30 μm spaced Pt interdigitated electrodes, patterned onto the Si_3N_4 surface, and on the other side a Pt resistor acting as a heater. The Si_3N_4 layer, grown by CVD onto a SiO_2 500 μm thick wafer, was characterized by a nanometric roughness of ± 2.5 nm, as determined by AFM microscopy. The electrical tests have been carried out at different operating temperatures (25, 50 and 75 °C) by recording the resistance of the NRs network, using a Keithley 2001 multimeter in dry air and in presence of different NO_2 gas concentrations (200 – 800 ppb range), obtained by diluting NO_2 gas (5 ppm in air) with dry air by an MKS147 multigas mass controller (MKS Instruments Inc.). A full colour 10 mm RGB (Kingbright) light-emitting diode set at 430 nm wavelength (purple-blu light) was used as irradiation source, producing an estimated light intensity of 0.70 mW/cm^2 with a 30 mm distance between the light source and the film.

4. Conclusions

We presented a new approach towards the synthesis of large-area sensing devices based on a bi-dimensional network of ZnO NRs. This approach is based on an all-solution method that couples a simple soft-lithographic procedure, applied to metal-loaded hydrogels, and aqueous hydrothermal growth of ZnO NRs. It involves the use of an extremely simple experimental setup and very inexpensive and environmentally benign chemical reactants. The method allows the formation of well connected networks of NRs over areas of several

square millimeters and it can be realized directly over a pattern of metal lines electrodes, allowing the fabrication of very stable, robust and inexpensive sensing devices. No alignment between the electrodes and the NRs patterns is required, reducing considerably the complexity of the microdevice fabrication. The design of the network forces the probing current to flow directly through the NRs, allowing to take full advantage of their sensing capabilities. In presence of UV irradiation good responses to NO_2 at trace levels (<100 ppb) and fast response times have been obtained even at temperatures between 25 and 75 °C.

Acknowledgments

This work was supported by Italian PRIN_09 Project N° 2009ALAX7Y "Sviluppo di materiali con architettura gerarchica per sensori di ossidi di azoto a bassa temperatura per il monitoraggio ambientale". Authors would like to thank Laboratorio Arvedi (University of Pavia, CISRiC) for the use of scanning electron microscope.

References

1. Z. Song, W. Helin, L. Yuhao, W. Wang, L. Hao, W. Haoning, Q. Pingli, Z. Wei and F. Guojia, *Ieee T Nanotechnol* , 2014, **13**, 167–171.
2. M. Hussain, A. Khan, M. A. Abbasi, O. Nur, M. Willander, *Micro Nano Lett*, 2014, 9, 539-543.
3. C. T. Pan, Y. C. Chen, C. C. Hsieh, C. H. Lin, C. Y. Su, C. K. Yen, Z. H. Liu, and W. C. Wang, *Sensor Actuat A-Phys* , 2014, **216**, 318–327.
4. D. Cammi, R. Röder, and C. Ronning, *J Phys D Appl Phys,* 2014, **47**, 394014
5. D. V. Quang , K. Do-Il, D. Le Thai, K. Bo-Yeong, H. Byeong-Ung, J. Mi, S. Kyung-Sik, K. Sang-Woo, and L. Nae-Eung, *Nanoscale*, 2014, **6**, 15144 –15150.
6. H. Muguerra, G. Berthoux, W. Z. N. Yahya, Y. Kervella, V. Ivanova, J. Bouclé, and R. Demadrille, *Phys Chem Chem Phys* 2014, **16**, 7472–7480
7. Z. Yuan, *J Mater Sci-Mater El* 2014, **25**, 2248–2252.
8. D. Y Son, J.-H. Im, H.-S. Kim, and N.-G. Park, *J Phys Chem C* 2014, **118**, 16567–16573.
9. M. Raja, N. Muthukumarasamy, D. Velauthapillai, R. Balasundaraprabhu, S. Agilan, and T.S. Senthil. *Sol Energy* 2014, **106**, 129–135.
10. J. Dai, C. Xu, J. Li, Y. Lin, J. Guo, and G. Zhu. *J Phys Chem C* 2014, **118**, 14542–14547
11. J. Kong, S. Chu, J. Huang, M. Olmedo, W. Zhou, L. Zhang, Z. Chen, and J. Liu, *Appl Phys A* 2013, **110**, 23–28.
12. Q.-M. Fu, W. Cao, G.-W. Li, Z.-D. Lin, Z. Chen, C.-B. Xu, Y.-F. Tu, and Z.-B. Ma, *Appl Surf Sci,* 2014, **293**, 225–228.
13. H. Jeong, D. J. Park, H. S. Lee, Y. H. Ko, J. S. Yu, S.-B. Choi, D.-S. Lee, E.-K. Suh, and M. S. Jeong, *Nanoscale* 2014, **6**, 4371–4378.
14. K. V. Gurav, M. G. Gang, S. W. Shin, U. M. Patil, P. R. Deshmukh, G. L. Agawane, M. P. Suryawanshi, et al., *Sensor Actuat B-Chem* 2014, **190**, 439–445.
15. J. Y. Kim, S.-Y. Jo, G.-J. Sun, A. Katoch, S.-W. Choi, and S. S. Kim, *Sensor Actuat B-Chem* 2014, **192**, 216–220.
16. S. J. Kwon, J.-H. Park, and J.-G. Park, J. *Electroceram*, 2006, **17**, 455–459.
17. M. Law, L. E. Greene, J. C. Johnson, R. Saykally, and P. Yang, *Nat Mater*, 2005, **4**, 455–459.
18. J. Qiu, X. Li, W. He, S.-J. Park, H.-K. Kim, Y.-H. Hwang, J.-H. Lee, and Y.-D. Kim, *Nanotechnology*, 2009, **20**, 155603.
19. J. Qiu, X. Li, F. Zhuge, X. Gan, X. Gao, W. He, S.-J. Park, Hyung-Kook Kim, and Y.-H. Hwang, *Nanotechnology*, 2010, **21**, 195602.
20. C. Xu, P. Shin, L. Cao, and D. Gao, *J. Phys. Chem. C*, 2010, **114**, 125–129.
21. M. Willander, O. Nur, Q. X. Zhao, L. L. Yang, M. Lorenz, B. Q. Cao et al, *Nanotechnology* 2009, **20**, 332001 pp. 1–40.
22. J. H. Park, P. Muralidharan, D. K. Kim, *Mater Lett*, 2009, **63**, 1019–1022.

23. S. Xu, and Z. L. Wang, *Nano Research,* 2011, **4**, 1013–1098.
24. R. B. Peterson, C. L. Fields, and B. A. Gregg, *Langmuir* 2004, **20**, 5114–5118.
25. Q. Huang, L. Fang, X. Chen, and M. Saleem, *J Alloy Compd* 2011, **509**, 9456–9459.
26. K. H. Tam, C. K. Cheung, Y. H. Leung, A. B. Djurišić, C. C. Ling, C. D. Beling, S. Fung, et al, *The J Phys Chem B*, 2006, **110**, 20865–20871.
27. Q. Li, J. Bian, J. Sun, J. Wang, Y. Luo, K. Sun, and D. Yu, *Appl Surf Sci*, 2010, **256**, 1698–1702.
28. D. Polsongkram, P. Chamninok, S. Pukird, L. Chow, O. Lupan, G. Chai, H. Khallaf, S. Park, and A. Schulte. *Physica B*, 2008, **403**, 3713–3717.
29. S.-W. Chen, and J.-M. Wu, *Acta Mater*, 2011, **59**, 841–847
30. M. N. R. Ashfold, R. P. Doherty, N. G. Ndifor-Angwafor, D. J. Riley, and Y. Sun, *Thin Solid Films* 2007, **515**, 8679–8683.
31. J. Qiu, X. Li, W. He, S.-J. Park, H.-K. Kim, Y.-H. Hwang, J.-H. Lee, and Y.-D. Kim, *Nanotechnology* 2009, **20**, 155603.
32. M. Law, L. E. Greene, J. C. Johnson, R. Saykally, and P. Yang, *Nat Mater* 2005, **4**, 455–459.
33. C. Xu, P. Shin, L. Cao, and D. Gao, *J Phys Chem C*, 2010, **114**, 125–129.
34. J. R. Morante, *Nanotechnology*, 2013, **24**, 444004.
35. G. Tulzer, S. Baumgartner, E. Brunet, G. C. Mutinati, S. Steinhauer, A. Köck, P. E. Barbano, and C. Heitzinger, *Nanotechnology*, 2013, **24**, 315501.
36. M. -Z. Yang, C. -L. Dai, and C. -C. Wu, *Sensors*, 2011, **11**, 11112–11121.
37. J. Gong, Y. Li, and Y. Deng, *Phys Chem Chem Phys*, 2010, **12**, 14864–14867.
38. S. H. Ko, I. Park, H. Pan, N. Misra, M. S. Rogers, C. P. Grigoropoulos, and A. P. Pisano, *Appl Phys Lett*, 2008, **92**, 154102.
39. Y. K. Park, H. S. Choi, J.-H. Kim, J.-H. Kim, and Y.-B. Hahn, *Nanotechnology*, 2011, **22**, 185310.
40. N. Liu, G. Fang, W. Zeng, H. Zhou, F. Cheng, Q. Zheng, L. Yuan, X. Zou, and X. Zhao, *ACS Appl Mater Interfaces*, 2010, **2**, 1973–1979.
41. M.-W. Ahn, K.-S. Park, J.-H. Heo, J.-G. Park, D.-W. Kim, K. J. Choi, J.-H. Lee, and S.-H. Hong, *Appl Phys Lett,* 2008, **93**, 263103. Da qui: solo nomi journal da abbreviare e rendere corsivi
42. M.-W. Ahn, K.-S. Park, J.-H. Heo, D.-W. Kim, K. J. Choi, and J.-G. Park, *Sens Actuators, B*, 2009, **138**, 168–173.
43. I. G. Tredici, A. Resmini, F. Yaghmaie, M. Irving, F. Maglia, and U. Anselmi-Tamburini, *Thin Solid Films*, 2012, **526**, 22–27.
44. I. G. Tredici, F. Yaghmaie, M. Irving, M. B. J. Wijesundara, F. Maglia, E. Quartarone, and U. Anselmi-Tamburini, *J Am Ceram Soc*, 2011, **94**, 3171–3174.
45. I. G. Tredici, F. Yaghmaie, M. Irving, M. B. J. Wijesundara, F. Maglia, E. Quartarone, P. Galinetto, and U. Anselmi-Tamburini, *Thin Solid Films*, 2011, **519**, 5854–5860.
46. I. G. Tredici, A. Resmini, S. Pin, P. Ghigna, T. Rovetta, M. Patrini, N. Rotiroti, M. Dapiaggi, and U. Anselmi-Tamburini, *J Phys Chem C*, 2013, **117**, 25108–25117.

47. V. Consonni, E. Sarigiannidou, E. Appert, A. Bocheux, S. Guillemin, F. Donatini, I.-C. Robin, J. Kioseoglou, and F. Robaut, *ACS Nano,* 2014, **8**, 4761–4770.
48. L. E. Greene, M. Law, D. H. Tan, M. Montano, J. Goldberger, G. Somorjai, and P. Yang, *Nano Lett,* 2005, **5**, 1231–1236.
49. H. Zhang, D. Yang, X. Ma, Y. Ji, J. Xu, and D. Que, *Nanotechnology,* 2004, **15**, 622.
50. X. Shan, X. Zhang, J. Gao, L. You, H. Xu, J. Xu, D. Yu, and H. Ye, *J Phys Chem C*, 2009, **113**, 18014–18019.
51. R. Yang and Z. L. Wang, *Solid State Commun,* 2005, **134**, 741–745.
52. T. Mahalingam, K. M Lee, K. H. Park, S. Lee, Y. Ahn, J.-Y. Park, and K.H. Koh, *Nanotechnology*, 2007, **18**, 035606.
53. C.-A. Lin, D.-S. Tsai, C.-Y. Chen, and J.-H. He, *Nanoscale,* 2011, **3**, 1195–1199.
54. T. Shinagawa, S. Watase, and M. Izaki, *Cryst Growth Des,* 2011, **11**, 5533–5539.
55. W. W. Li, W. L. Yu, Y. J. Jiang, C. B. Jing, J. Y. Zhu, M. Zhu, Z. G. Hu, X. D. Tang, and J. H. Chu, *J Phys Chem C*, 2010, **114**, 11951–11957.
56. J. Yi, J. M. Lee, and W. I. Park, *Sens Actuators, B*, 2011, 155, 264–269.
57. Y. Sun, G. M. Fuge, and M. N. R. Ashfold, *Chem Phys Lett,* 2004, **396**, 21–26.
58. B. Lin, Z. Fu, and Y. Jia, *Appl Phys Lett,* 2001, **79**, 943.
59. L.-Y. Chen, Y.-T. Yin, C.-H. Chen, and J.-W. Chiou, *J Phys Chem C*, 2011, **115**, 20913-20919.
60. S.-W. Fan, A. K. Srivastava, and V. P. Dravid, *Sens Actuators, B*, 2010, **144**, 159–163.
61. S.-W. Fan, A. K. Srivastava, and V. P. Dravid, *Appl Phys Lett*, 2009, **95**, 142106.
62. Q. Geng, Z. He, X. Chen, W. Dai, and X. Wang, *Sens Actuators, B*, 2013, **188**, 293–297.
63. Y.-J. Choi, I.-S. Hwang, J.-G. Park, K. J. Choi, J.-H. Park, and J.-H. Lee, *Nanotechnology*, 2008, **19**, 095508.
64. N. Barsan, U. D. O. Weimar, *J Electroceram*, 2002, **7**, 143–167.
65. H.-J. Lim, D. Y. Lee, Y.-J. Oh, *Sens Actuators, B*, 2006, **125**, 405–410.
66. C. Zhang, A. Boudiba, P. De Marco, R. Snyders, M.-G. Olivier, M. Debliquy, *Sens Actuators, B*, 2003, **181**, 395–401
67. S.-W. Fan, A. K. Srivastava, V. P. Dravid, *Appl Phys Lett*, 2009, **95**, 142106.
68. J. T. Yates, *Surface Science*, 2009, **603**, 1605–1612.

Figures

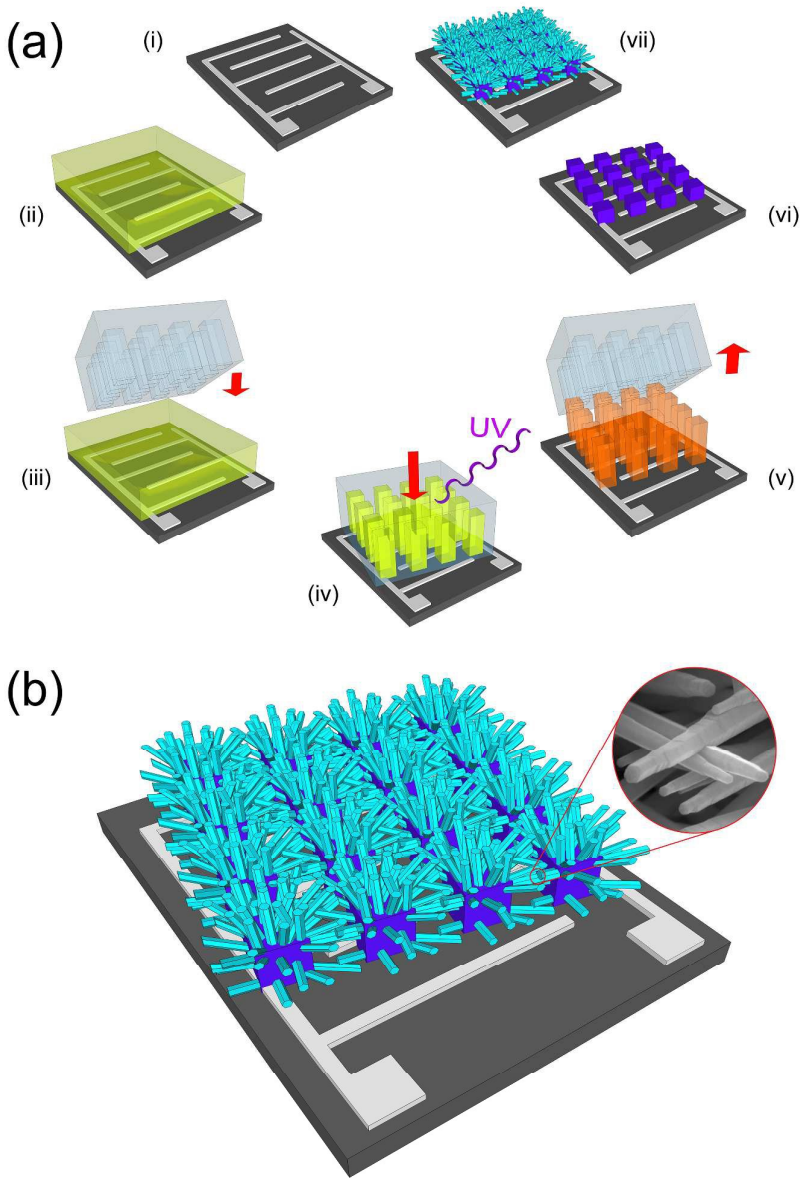

Figure 1. (a) Schematics of the fabrication process for the ZnO NRs network: (ii) deposition of a film of zinc-loaded hydrogel precursor by spin coating; (iii) casting of a PDMS mold; (iv) UV photo-polymerization of the precursor while applying a uniform load over the mold; (v) peeling of the PDMS mold; (vi) thermal degradation of the zinc-loaded hydrogel pattern; (vii) hydrothermal growth of the ZnO NRs. (b) Schematics of a functional device realized by growing the network of NRs on Pt interdigitated electrodes. Inset: SEM micrograph showing a detail of the bridging NRs.

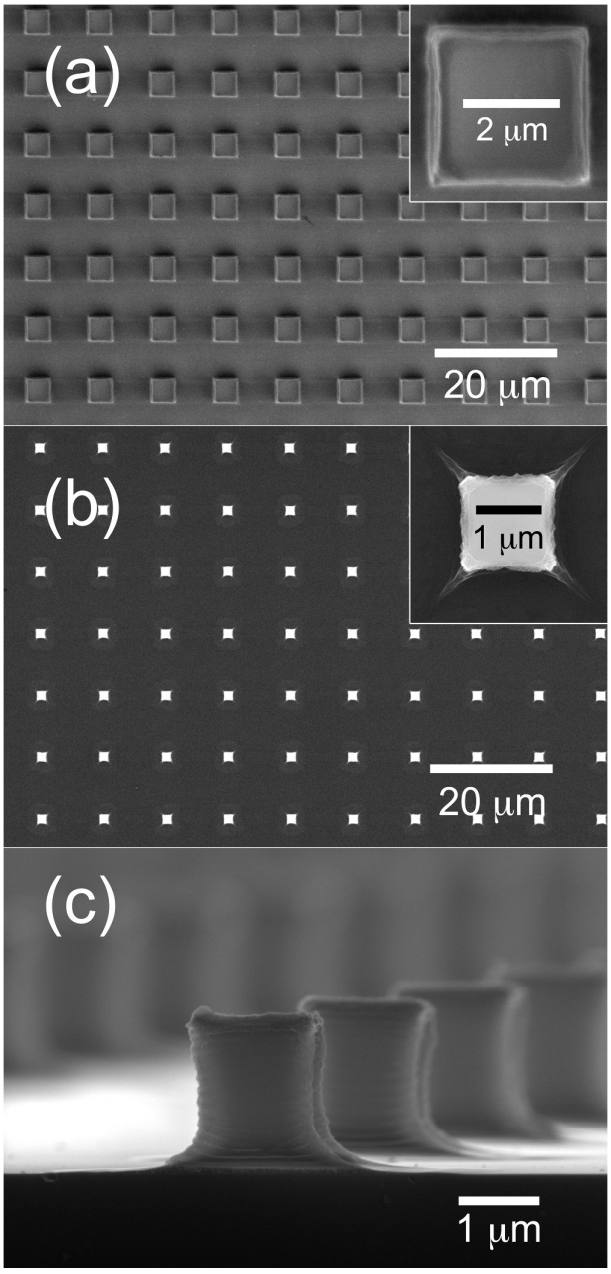

Figure 2. Formation of the ZnO seed micropillars. (a) Top-view of the patterned hydrogel precursor after the soft-lithography process (micromoulding) presenting micro-pillars with a size of about 3.5 x 3.5 x 10 μm; (b) top-view of the same pattern after thermal degradation at 500 °C for 1 h; (c) Vertical view of an enlarged detail of the ZnO micropillars, obtained after thermal degradation, with a dimension of about 1 x 1 x 2 μm.

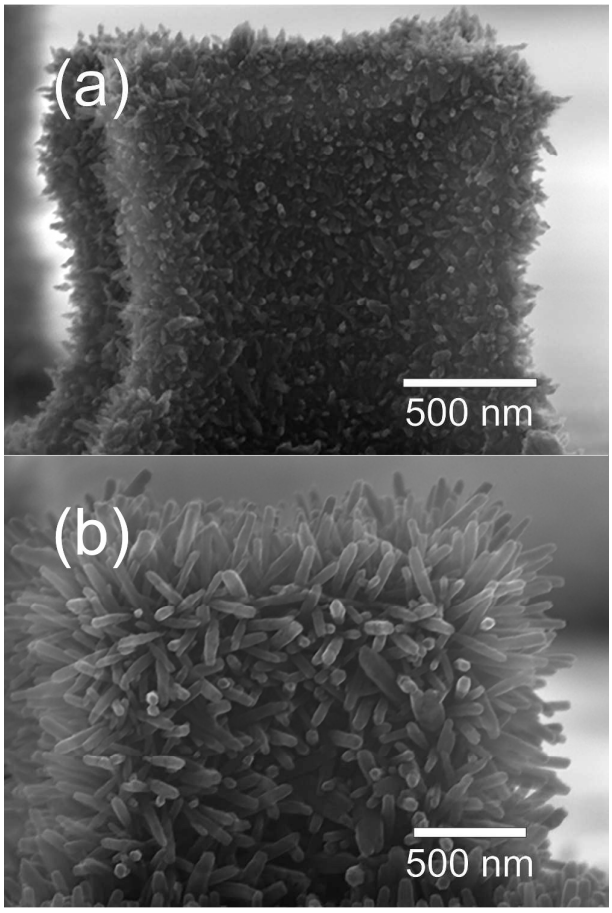

Figure 3. Early stages of the NRs hydrothermal growth onto the surfaces of a ZnO micropillar.

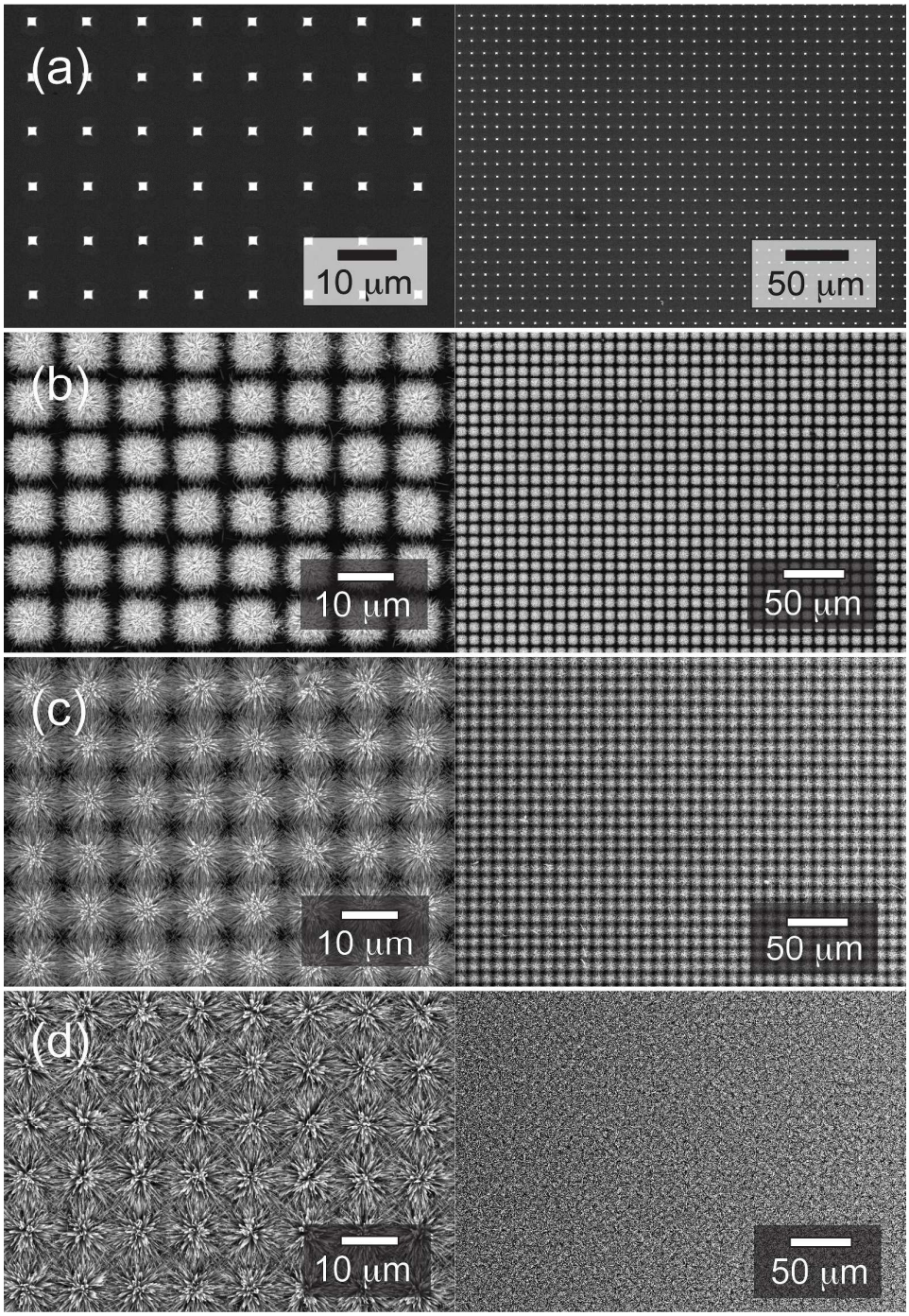

Figure 4. SEM micrographs showing top-views of the NRs growth process at two different magnifications (left side: 3000 x, right side: 750 x). The images show the patterned ZnO micro-pillars (a) and the ZnO NRs after 135 (b), 180 (c) and 300 min (d) of growth.

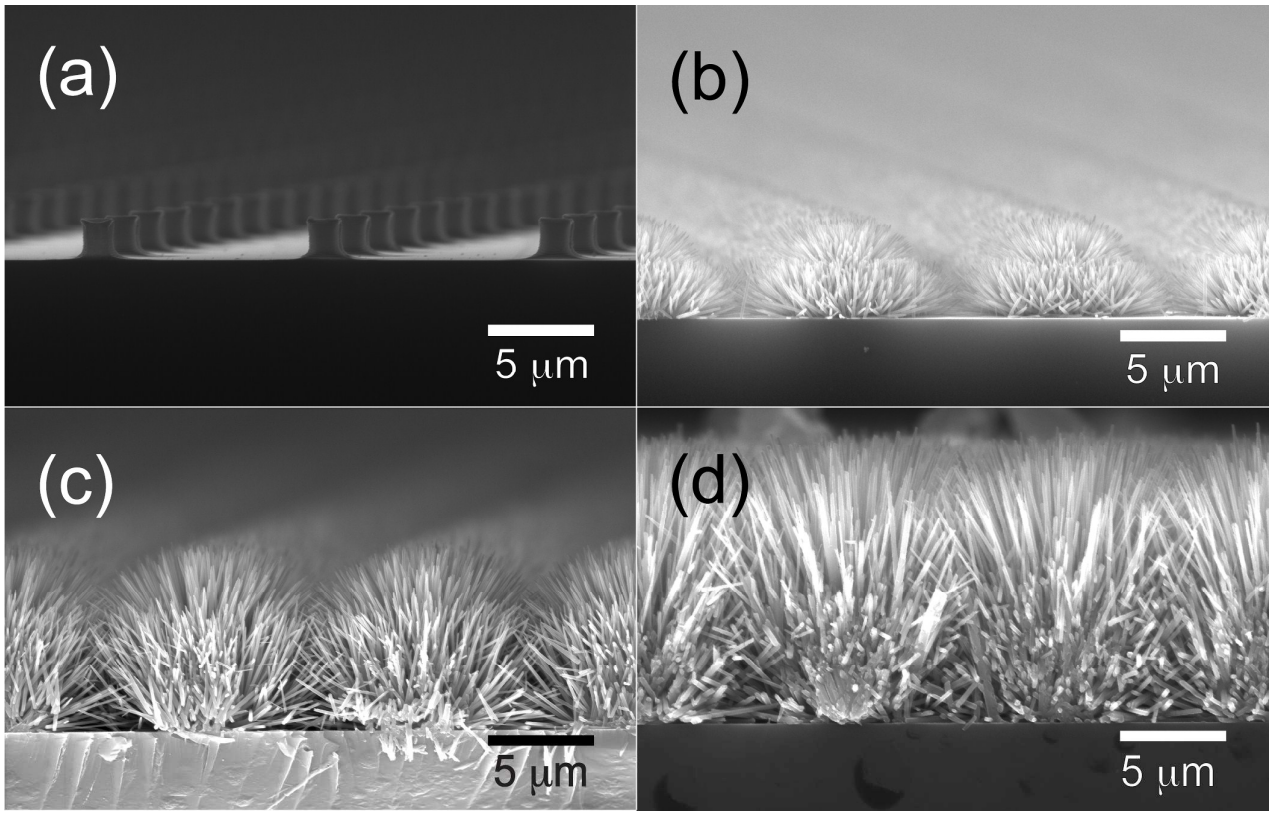

Figure 5. Cross-sections of the same samples of Figure 4. The images show the patterned ZnO micro-pillars (a) and the ZnO NRs after 135 (b), 180 (c) and 300 min (d) of growth.

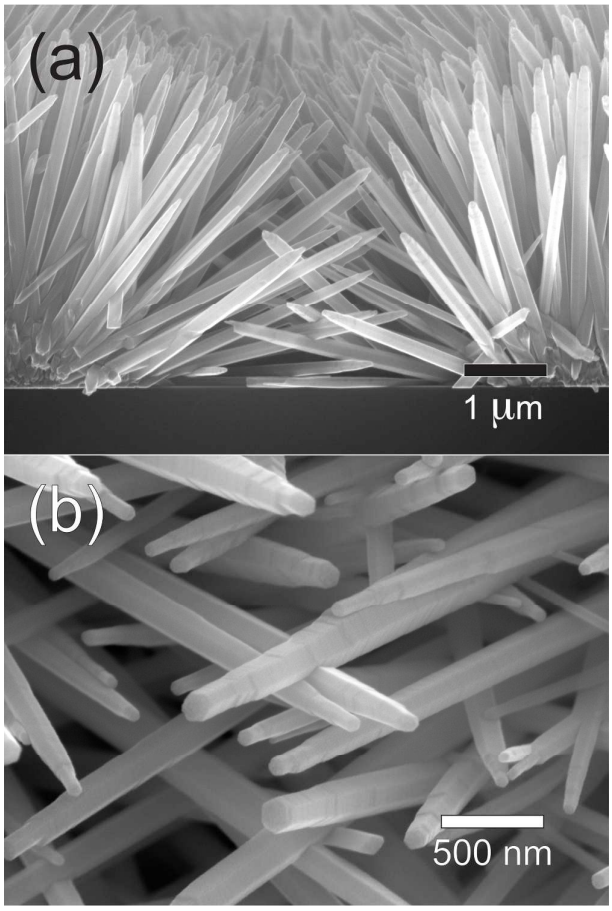

Figure 6. Enlarged views of the samples reported in Figure 4 and Figure 5 showing the connections between the NRs that grow from neighboring ZnO micropillars: (a) cross-section; (b) top view.

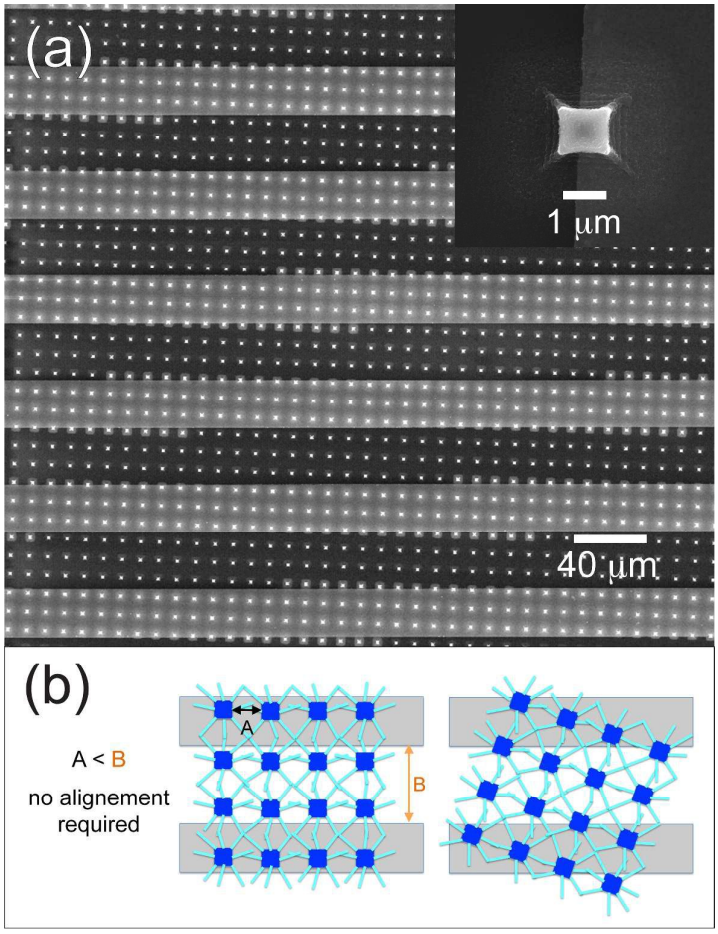

Figure 7. (a) Top-view of a ZnO seeding pattern prepared over Pt interdigitated electrodes: the pattern is not aligned with the electrodes; despite that, a conduction path along the NRs is always possible as long as the distance between the micropillars is smaller that the pitch between the metal lines. Inset: example of a pillar of ZnO deposited across the edge of a Pt line of the interdigitated electrodes. (b) Scheme that shows how such a final ZnO NRs network allows to establish electrical contact between adjacent electrodes, no matters what is the alignment of the ZnO seed layer patterned through soft-lithography.

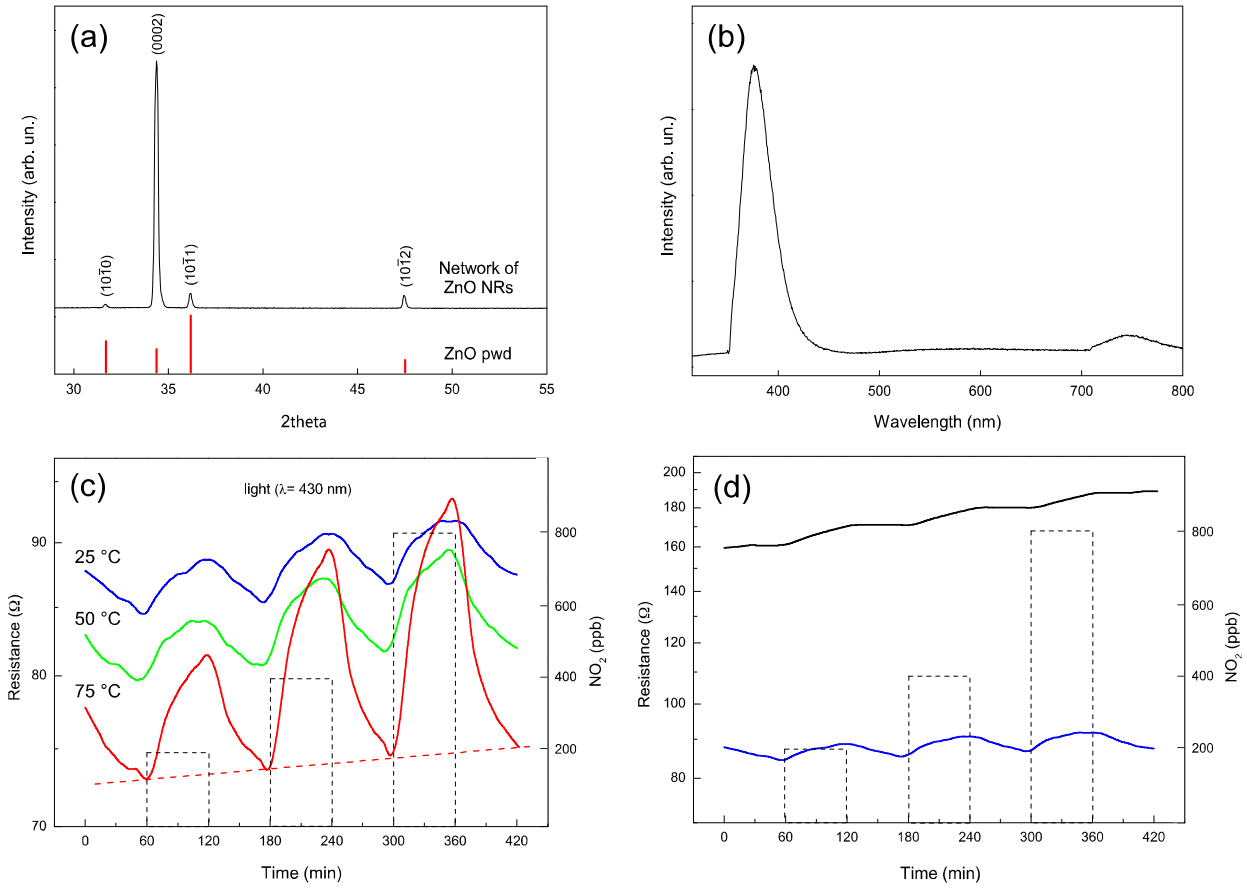

Figure 8. Structural, optical and electrical characterizations of an as-grown network of ZnO NRs. (a) X-rays diffraction pattern and (b) room-temperature PL spectrum. (c) photoelectrical induced resistance modulation at 430 nm purple-blue light wavelength of the ZnO structures at different temperatures. Base line resistance in air at 75 °C is displayed by the red horizontal dashed line. NO_2 pulses at 200, 400 and 800 ppb are represented by the vertical dotted rectangular boxes. (d) room-temperature comparison of the electrical response to NO_2 of the ZnO nanostructures, in dark and under irradiation with a 430 nm purple-blue light.

Temperature	200 ppb NO_2	400 ppb NO_2	800 ppb NO_2
25°C	4.76 ± 1.04	6.18 ± 1.67	5.75 ± 1.52
50°C	5.59 ± 1.16	8.27 ± 1.34	9.75 ± 1.73
75°C	11.55 ± 1.53	21.4 ± 2.23	25.33 ± 3.22

Table 1: Sensitivity Response (SR) as represented by the ratio: SR = [(Rg – Ra)/Ra)]·100 of the network of ZnO NRs in the temperature range 25 - 75 °C and different gas concentrations (200 – 800 ppb NO_2) under purple-blue light (430 nm wavelength).

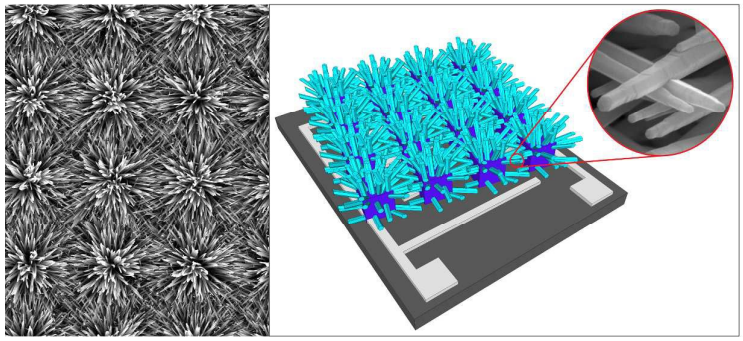

Soft-lithography of Zn-loaded hydrogels and a subsequent hydrothermal growth process yield self-assembling networks of bridging nanorods (NRs). The NRs are grown on a bi-dimensional pattern of seeding micropillars of ZnO until they get in touch each other forming junctions that provide a preferred electrical path for the operative current of functional devices. In order to prove the establishment of such electrical path between electrodes through NRs junctions, the device is tested as a gas sensor for NO_2 at ppb trace level.